IEEE Access
Multidisciplinary | Rapid Review | Open Access Journal

Received 9 February 2024, accepted 22 March 2024, date of publication 9 April 2024, date of current version 18 April 2024.

Digital Object Identifier 10.1109/ACCESS.2024.3386554

RESEARCH ARTICLE

Object Weight Perception in Motor Imagery Using Fourier-Based Synchrosqueezing Transform and Regularized Common Spatial Patterns

NEDIME KARAKULLUKCU[1], FATİH ALTINDİŞ[1,3], AND BÜLENT YILMAZ[2,3]
[1]Electrical and Computer Engineering Department, Abdullah Gül University, 38080 Kayseri, Turkey
[2]Electrical Engineering Department, Gulf University for Science and Technology, Hawally 32093, Kuwait
[3]Electrical-Electronics Engineering Department, Abdullah Gül University, 38080 Kayseri, Turkey

Corresponding author: Nedime Karakullukcu (nedime.ozturk@agu.edu.tr)

This work was supported in part by Scientific and Technological Research Council of Turkey (TÜBİTAK) under Project 119E120. The work of Nedime Karakullukcu was supported in part by the Higher Education Council (HEC) of Turkey 100/2000 Ph.D. Scholarship Program, and in part by the 2211-A National Ph.D. Scholarship Program. The APC of this paper was covered by Gulf University for Science and Technology, Kuwait.

This work involved human subjects or animals in its research. Approval of all ethical and experimental procedures and protocols was granted by the Erciyes University Ethics Committee (January 9, 2019, 2019/32), Kayseri, Turkey.

ABSTRACT This study addresses the challenge faced by individuals with upper-limb prostheses in regulating grip force and adapting movements to different object weights. Despite limited exploration, this research pioneers the use of EEG to estimate object weight perception in the context of upper-limb prostheses. Investigating neural correlates in this population provides valuable insights and aids the development of neurofeedback-based strategies for weight perception. Our objective is to identify EEG features predicting the weight perception of held objects. Employing Fourier-based synchrosqueezing transform (FSST) and regularized Common Spatial Patterns (CSP) features, we classify motor imagery waves representing three weight categories (light, medium, heavy). Subjects perform actual motor tasks before imagery sessions, and our approach integrates EEG features of both movements to train subject-specific machine learning models. Results reveal that FSST- singular value decomposition (SVD) features for medium and heavy objects are most distinctive. Achieving up to 90% accuracy, spatial features demonstrate effective classification of motor imagery for different weights. Unlike weight prediction studies, our focus is on visual perception and imagination of object weights, enhancing prosthetic hand system preconditioning. Binary classification surpasses 70% accuracy in predicting object weights, uniquely utilizing actual movement data for CSP algorithm regularization coefficient estimation.

INDEX TERMS Brain computer interfaces, common spatial pattern (CSP), EEG signal processing, Fourier-based synchrosqueezing transform (FSST), weight perception.

I. INTRODUCTION

Accurate perception of the weight of objects is crucial for the individuals utilizing upper-limb prostheses to interact with their environment effectively. The prostheses used especially for the upper extremity differ according to the level of amputation, just as the methods used to move the prosthesis. In some prosthesis types, only cosmetic use is prominent, whereas in others, the prosthetic hand is opened and closed by the individual's own movements, e.g., moving the shoulder. As for the myoelectric prosthesis, arm and hand movements are performed with the muscle signals received from the electromyography (EMG) electrodes placed in the appropriate places (on the skin) of the amputated limb [1], [2].

Alternatively, integration of electroencephalography (EEG) signal analysis for the control of the prosthesis is

The associate editor coordinating the review of this manuscript and approving it for publication was Gyorgy Eigner.

possible. Numerous studies have demonstrated the potential of EEG in decoding various aspects of motor control and perception, including studies on motor imagery [3], [4], [5], [6], [7], [8], emotion recognition [9], sleep stage classification [10], tactile perception [11], attention training [12] and brain-computer interface (BCI) game development [13], [14], [15]. In fact, efforts have been made to use electroencephalography (EEG) signals for controlling the upper extremity prosthesis [16], [17], [18], [19]. In [20], they investigate the utilization of EEG for controlling a prosthetic hand for enhancing the quality of life for individuals with physical or motor. They employ the EEGNet, a convolutional neural network, for feature extraction and signal classification across five motor-imagery hand tasks performed by users. In [21], 3-finger anatomical robot hand model is developed for handicapped people. Eight channel motor imagery EEG data from primary motor cortex is used to control (flexion and extension) the robot hand. Frequency domain features of EEG are used for operating the prosthetic arm in [22]. In another attempt, the natural resting-state functional connectivity in the brain is investigated to predict how well an individual could adapt their right (dominant) upper limb's motor skills when faced with a robot-controlled force field during reaching tasks [23]. Recently, in [24], the possibility of using EEG to detect both the motion and the varying weights that a person is lifting is studied. They collected EEG data while performing biceps flexion-extension movements under various weight conditions, including lifting with no weight (empty), medium weight, and heavy weight.

Even though prosthetic devices offer remarkable functionality, they often lack the ability to provide real-time feedback on the weight of the grasped objects. Consequently, individuals with upper-limb prostheses may struggle to regulate their grip force and adequately adapt their movements to different object weights [25]. The use of EEG to estimate the weight of objects to be carried specifically in the context of upper-limb prostheses remains largely unexplored. Investigating the neural correlates of weight perception in individuals that use prosthetic limbs can offer valuable insights into the underlying mechanisms and help the development of neurofeedback-based strategies for weight perception. Therefore, the objective of this study is to seek distinctive features of EEG signals to predict the weight perception of the objects held by the individuals. The research methodology is visualized in Fig. 1, which depicts the sequential steps involved in utilizing EEG signals for predicting weight perception of an object in individuals with upper-limb prostheses.

We find research groups in the literature that work on their unique datasets focused on weight prediction. In [26], researchers designed a study to determine the brain's perception of weight based on 4-channel EEG signals obtained when participants applied pressure corresponding to different weight levels to their hands (as a type of haptic application). They used the relative power values of the alpha and beta subbands of EEG signals for the classification of weight-bearing and resting states. In another study, 32-channel EEG signals

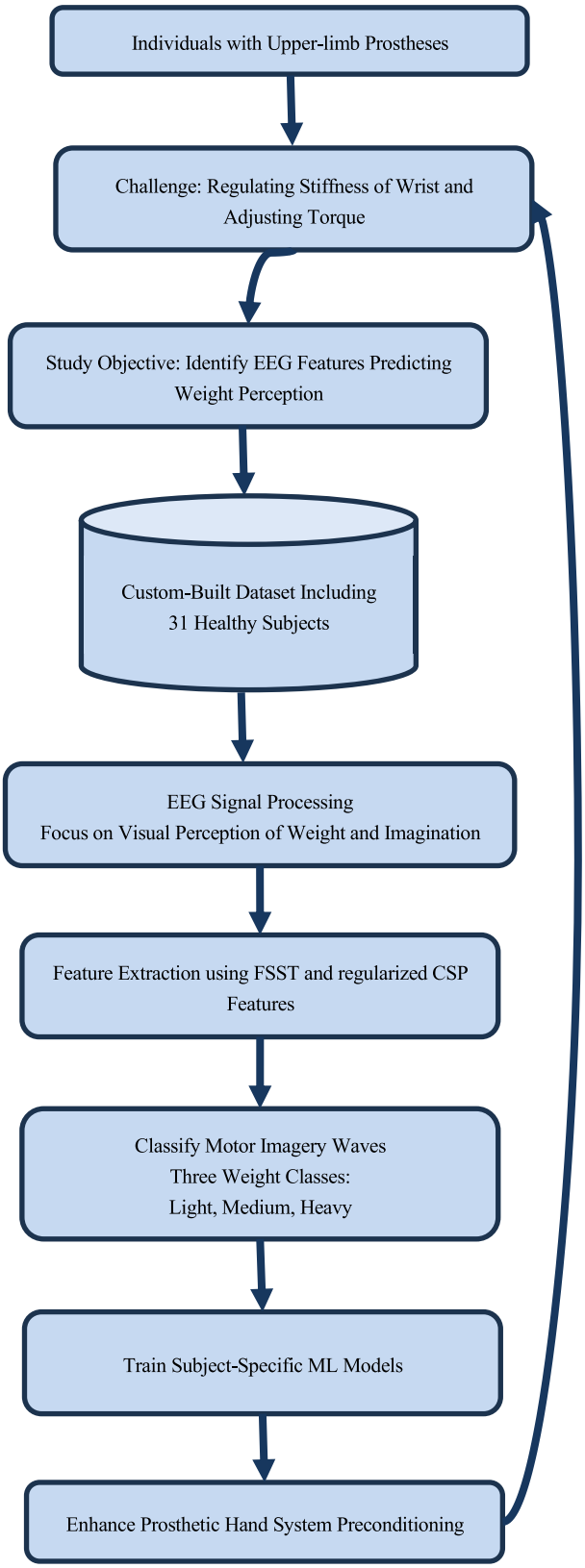

FIGURE 1. Flowchart illustrating the process of EEG-based weight perception prediction.

and EMG signals from five arm and hand muscles are collected from participants [27]. Subjects randomly grasped and

lifted a series of lightweight or heavy objects and guessed the weights. They reported the effect of the bias in weight perception based on previous lifting experience and its relationship with force scaling. In [28], a comprehensive study for using brain signals during the execution of grasping and lifting functions by a robot arm is studied (using the hand of a small Nao robot). In [29], the motor imagery signals are obtained from 129-channel EEG data during the grasping and lifting of a glass of water by 28 participants [29]. Three-class classification problem is posed as grasping, lifting, and grasping+lifting. They used band power values of 8-14 Hz subband from 500 ms epochs and reported 95% classification accuracy. However, they also reported that the classification accuracy significantly decreased in continuous prediction.

Here we briefly introduce methods that are found a broad use from the signal processing community for analyzing EEG signals. The reader is referred to related studies for the detailed explanation of the discussed methodologies since it is beyond the scope of this study. The simplest statistical features of EEG signals such as mean, variance, skewness etc., provide discriminative information about sleeping and resting state of the person [30]. Hjorth parameters are the variance of derivatives of EEG signals – mobility, activity, complexity – widely used features to describe characteristics of EEG signals [31], [32]. Shannon's entropy, fractal dimensions, topological data analysis and Hurst and Lyapunov exponents are mainly known as nonlinear features. In EEG analysis such features are estimated by embedding EEG signals to an attractor [33], [34]. Frequency-domain features e.g., power spectral density (PSD), frequency bands (delta 0.5-4 Hz, theta 4-7 Hz, alpha 8-13 Hz, beta 13-30 Hz) and ratios of frequency bands extensively used features of EEG signals [35].

Various methods for extracting features from EEG signals to distinguish between different cognitive states have been explored extensively. In this context, one of the methods employed is the short-time Fourier transform (STFT). STFT is commonly used in the EEG signal processing community. STFT method divides EEG signals into segments/windows to analyze them as if they were stationary signals. In [36], two deep learning pipelines utilizing Convolutional Neural Networks (CNN) and Long Short-Term Memory (LSTM) are used for the classification of motor imagery tasks. Frequency domain representations from EEG signals are extracted with STFT and fed into pipelines for training the models. Feature selection from STFT covariances are proposed to extract spatial, time and frequency features concurrently in [37]. Since EEG signals inherently exhibit non-stationary characteristics, synchrosqueezing transform (SST) provides a better time-frequency representation for the feature extraction as compared to STFT [38], [39], [40], [41], [42]. SST is suitable for generating a localized time-frequency (TF) representation of nonstationary signals. In [41], a novel approach is introduced for emotion classification using EEG signals. This approach incorporates singular value decomposition (SVD) and multivariate SST. In another study, emotion recognition methodology that relies on multivariate SST analysis on multichannel EEG data [43]. Precise TF localization of SST is also convenient for the epileptic seizure detection as reported in [42]. In EEG based BCI framework, time-frequency coherence using STFT and SST methods are found between electrophysiological signals.

Another methodology employed in the context of motor imagery based BCIs is common spatial pattern (CSP) filtering [44], [45]. CSP filters maximize the variance of one class, whereas minimize the variance of the other class. CSP filtering is one of the *state-of-the-art* methods for feature extraction from EEG signals, especially when the binary-class motor imagery problem is posed. CSP aims to enhance the discriminative power of EEG signals by transforming them into spatial patterns that highlight the differences between different cognitive states or tasks. CSP filters are highly sensitive to noise and tend to overfit the training set. Thus, it results in poor decoding performance when tested on cross session/subject data. To address this limitation, alternative CSP algorithms have been suggested. Subband common spatial pattern (SBCSP) performs CSP on the subbands of EEG data [46], filter bank common spatial pattern (FBCSP) selects features from various frequency subbands according to the maximal mutual information criterion [47]. Additionally, CSP filter regularization approaches are proposed in the literature for improving the cross session/subject performance [48], [49]. In [50], the weighted sum of covariance matrices of other sessions/subject are used for regularization of the spatial filters. In [51], two step regularization is applied to spatial filters for reducing training set bias especially when small set of training trials are available.

Here in this study, we use features of time domain, frequency domain, time-frequency domain and CSP methods to create feature vectors [36], [39], [44], [45], [46], [47], [52], [53], [54], [55]. The rest of this paper is organized as follows. The experimental paradigm and structure of the custom-built EEG dataset and the methods used to extract features are presented in Section II. Experimental results are given in Section III. The discussion of the results is given in Sec. IV.

II. MATERIALS AND METHODS

A. EXPERIMENTAL SETUP AND DATASET

Experiments are conducted in Biomedical Image and Signal Analysis (BISA) Laboratory of Abdullah Gul University, Kayseri, Turkey. In total, 31 volunteers joined the experiments (mean age: 22 years, age range: 19-35). Subjects reported no history of neurological diseases. The experiments are approved by the Erciyes University Ethics Committee (January 9, 2019, 2019/32), Kayseri, Turkey. Gold alloy dry electrodes (g.Sahara) and the wireless EEG signal amplification system (g.Nautilus) are used in the experiments. EEG records are taken from 16 channels located at Cz, FP2, F3, Fz, F4, T7, C3, FP1, C4, T8, P3, Pz, P4, PO7, PO8, and Oz electrode positions according to the 10-20 international system [56]. The reference electrodes are attached to left and right antitragus (behind the ear). The sampling rate is

set to 500 Hz and the records are filtered using an analog bandpass filter (2-200 Hz) and an analog notch (50 Hz) filter.

Experiment setup consists of two sessions, actual movement and imagery movement. There are five phases in the actual movement session: resting phase, holding phase, lifting-up phase, putting-down phase, and relaxation phase. In the rest phase, a red circle is presented in the middle of the plus sign for 2.5 s. The subjects fix their eyes on the circle during this phase. In the holding phase, one of the three visual cues each representing one of three bottle each with a different weight (light, medium, heavy) is showed for 0.5 s to the subjects. Next, subjects reach and grasp the cued bottle without lifting it up. One second is allocated for subjects to reach and grasp the bottle. In the lifting-up phase, an upside arrow is shown on the screen for 2 seconds. Subjects lift up the bottle approximately 20 cm above the desk level and keep holding the bottle in this position until the next cue. When a down-arrow cue is given, subjects put down the bottle to its initial position. Then subjects rest for 2 seconds before the new trial begins. Subjects perform 30 trials (10 for each bottle) in the actual movement session.

The second session -imagery movement- subjects asked to perform imagination of the lifting up and putting down of the bottles. In this session, trials consist of four phases: resting, visual cue, imagination, and relaxation. The resting and visual cue phases are the same as the former session apart from duration of the cue appearance. Unlike the actual movement session, subsequently after the cue subjects start imagining the lifting up and putting down movements of the given cue. After 3 seconds of imagination phase, relaxation phase of 2 seconds ends one trial of imagination. Subjects perform 30 imagination trials (10 for each bottle).

The actual movement session was designed and implemented to facilitate participants' imagery of movement during the imagery movement session. Initially, participants engaged in actual movements and experienced the weight of objects, with the aim of enabling them to comfortably imagine the movements during the subsequent session.

The experimental paradigm of both sessions is shown in Fig. 2. In both sessions, each of the cues is given in random order. Between two sessions, a minimum 15-min break is given to subjects in order to minimize fatigue. Bottle weights are 25 gr, 523 gr, and 1037 gr for light, medium, and heavy respectively. There are 924 trials for actual movement session and 924 trials for motor imagery session in total.

B. PREPROCESSING

We preprocessed the recordings using EEGLAB (v2021.0) tools in MATLAB (R2019a) in order to remove blink artefacts. Independent component analysis (ICA) is applied to each session and eye blink related components are manually removed from the data. After the blink removal, 5th order digital Butterworth band-pass filter (8-30 Hz) is applied to data.

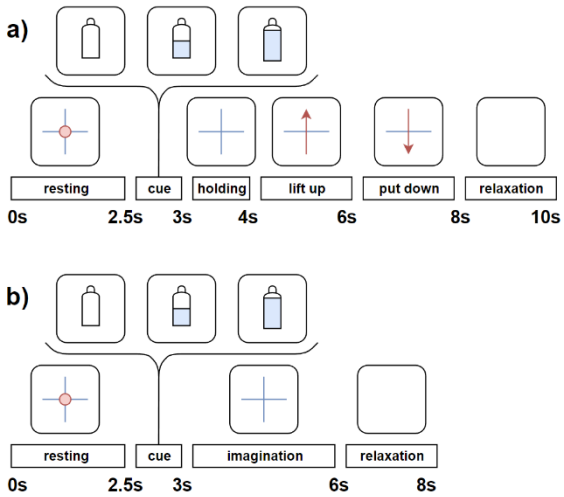

FIGURE 2. The experimental paradigm. (a) Actual movement session. (b) Imagery session.

C. FEATURE EXTRACTION / SELECTION

We use time domain, frequency domain, time-frequency domain and regularized CSP methods for feature extraction in MATLAB (2019a).

In this study, we first conducted feature extraction to the signals from 2.5 s - 5.5 s (visual cue and imagination phase) of imagery session. Afterwards, to explore the effect of actual movement session on the predicting of the weight perception, we employed a new method that includes the data from the 4 s – 6 s (lifting phase) of the actual movement session.

1) STATISTICAL AND TIME DOMAIN FEATURES

In order to investigate the feasibility of statistical methods, skewness, log energy entropy, Shannon entropy, kurtosis, and energy were used.

Skewness is a measure of the asymmetry of the corresponding probability distribution [56], [57]. In the context of analyzing EEG (Electroencephalogram) signals, skewness can be used as a feature to describe the shape of the signal's amplitude distribution [57].

Entropy is about how much information a signal carries. Entropy can be used to describe the complexity or irregularity of the brain activity [58]. The study conducted two different types of entropy measures: Shannon entropy (ShanEn) and log energy entropy (LogEn). Shannon entropy measures the uncertainty or information content in a dataset, whereas log energy entropy measures the distribution of energy across different frequency bands. The formulas for ShanEn and LogEn can be introduced with equation (1) and (2), respectively [59].

$$ShanEn(x) = -\sum_{i=0}^{N-1} (p_i(x))^2 (log_2(p_i(x)))^2 \quad (1)$$

$$LogEn(x) = -\sum_{1=0}^{N-1} (log_2(p_i(x)))^2 \quad (2)$$

where p_i represents the probability distribution function, and i indicates one of the discrete states.

Kurtosis is a measure of the difference between the highest value of the probability distribution and the highest value of the normal distribution of a random variable with real values, and it can be used to describe the ''fatness'' of the tails found in probability distribution of amplitudes in analyzing EEG signals [60].

In the context of EEG signal processing, energy is often computed to measure the total energy or power in a specific frequency band or across the entire signal. The formula for calculating energy in an EEG signal depends on the specific context and the desired frequency range. In a time-domain EEG signal to calculate the total energy, each data point in the EEG signal is squared and then all squared values are summed up [61].

AR modelling is adapted to EEG data as a time domain feature, and the means of the AR coefficients from each channel are extracted as features. In this approach, the best AR order, 4, is selected by trial and error [62].

All the features are calculated with MATLAB built-in functions. We applied these features separately for each of the 16 channels. Therefore, 6 features were extracted from each channel as statistical and time domain features.

2) FREQUENCY DOMAIN FEATURES

Another feature extraction method used for MI-based BCI is the power spectral density (PSD) in which the Welch method with a Hamming window is employed. The window is used to obtain eight segments of input signal with 50% overlapping between samples, and all segments are averaged to obtain a smoothed estimation. Additionally, this method is preferred to estimate the power at chosen frequency bands, the range between 8-12.5 Hz (mu band) and 13-30 Hz (beta band). We used the mu band power and the beta band power as features. Moreover, the band power ratios of the mu and beta activity, which is called relative band power, served as the additional feature. The methods were applied to each channel separately, and 4 features were extracted from each channel as frequency domain features.

3) TIME-FREQUENCY DOMAIN FEATURES

Different EEG signal frequency bands contain different information about the MI. In order to decompose a signal in multiresolution frequency and time, discrete wavelet transform (DWT) and Fourier-based synchrosqueezing transform (FSST) is used in this study. In DWT, Daubechies 4 is the wavelet function, and the wavelet decomposition level is determined automatically using MATLAB. The mean of the absolute values of detail coefficients corresponding to frequencies ranging from 7.8 Hz to 15 Hz are utilized as a feature obtained from the Discrete Wavelet Transform (DWT). We refer statistical, time domain, and frequency domain feature extraction methods explained so far as ''S-T-F-TF'' in the reminder of the article.

TABLE 1. The algorithm to calculate the FSST coefficients with the SVD as a dimension reduction method.

Algorithm 1: *FSST-SVD* ***Input****: Processed EEG signals* ***Window:*** *Kaiser* ***Window Length:*** *256* ***Selected Frequency:*** *8-30Hz*	**Output**
1. Apply FSST to each channel	*128x500 complex*
2. Select interested frequencies	*11x500 complex*
3. Calculate absolute values of the coefficients	*11x500 double*
4. Apply SVD to each channel.	*A: 11x500* *U: 500x500* *V: 11x11* *S: 500x11*
5. Exclude extra rows of zeros in S for the economy-size decomposition	*S:11x11*
6. Select the diagonal values of S	*S: 1x11*
7. Gather the 16 channels features	*s: 1x176 (11x16)*

EEG is a non-stationary signal whose spectral characteristics change with time. The short-time Fourier transform (STFT) and continuous wavelet transforms (CWT) have a deficiency in linear projection for non-stationary signals [40]. On the other hand, FSST is effective for a sharpened time-frequency representation. We previously demonstrated the contribution of FSST in the detection of motor intention [38]. We recommend consulting References [63] and [64] for the fundamental principles and theoretical aspects of FSST. Additionally, the singular value decomposition (SVD) algorithm was performed after applying FSST to reduce the dimensionality of the output of FSST and to extract significant features from the FSST coefficients [41]. The process is also summarized in the algorithm provided in Table 1. According to the algorithm, FSST was applied to individual EEG channels, generating complex number coefficients. To compute these coefficients, a Kaiser window of 256 units in length was employed to ensure accurate frequency resolution, resulting in a 128 $\times$ 500 matrix for each channel. After that, since the frequency range of interest was 8-30 Hz, the size of the matrix obtained from the FSST, which represents 128 frequencies, was reduced to 11 $\times$ 500 by selecting only the frequencies within the range of interest. Then, the absolute values of the coefficients for each channel were calculated and then these values were normalized.

Next, to reduce dimensionality of features extracted from the FSST coefficients, we use singular value decomposition

(SVD) method as follows,

$$\boldsymbol{A} = \boldsymbol{U} \times \boldsymbol{S} \times \boldsymbol{V}'. \tag{3}$$

In (3) **A** represents the coefficient matrix m x n, **U** signifies the m x m complex matrix, **V** denotes the n x n complex unitary matrix, and **S** takes the form of a diagonal matrix with singular vectors in a m x n configuration. In our study, we removed additional rows of zeros from **S** to achieve a more efficient decomposition, resulting in singular vectors arranged in an 11 × 11 configuration. We then considered the diagonal values of S as features (totaling 11), generating a 1 × 176 matrix for each of the 16 channels during a single trial of a subject.

4) REGULARIZED CSP FEATURES

Let $l \in \{1, \ldots, L$ be the index of trials and let $k \in \{1, \ldots, K$ be the index of classes. Then, we represent each trial as $\mathbf{X}_{lc} \in R^{NxT}$, with N and T channels are the number of channels and the number of time samples, respectively. Then, we calculate sample covariance matrix of each class

$$\mathbf{C}_k = \frac{1}{L} \sum_{l \in L} \mathbf{X}_{lk} \mathbf{X}_{lk}^T. \tag{4}$$

Note that EEG signals are bandpass filtered, and they are zero mean. As formally known, CSP uses spatial filters w to maximize variance of one class, whereas w minimizes the variance of the other class following [65]

$$J_{CSP}(\mathbf{w}) = \frac{\mathbf{w}^T \mathbf{C}_1 \mathbf{w}}{\mathbf{w}^T \mathbf{C}_2 \mathbf{w}}. \tag{5}$$

Following the methodology described in [48], we use regularization coefficients for estimating generalized covariance matrices. Regularization is completed in two steps; regularization of the sample covariance matrices and regularization of the CSP function $J_{CSP}(\mathbf{w})$. Equations (5) and (6) show regularization of the initial spatial covariance matrices estimated for a given class according to [48].

$$\hat{\mathbf{C}}_k = (1-\beta)\, s\mathbf{C}_k + \beta \mathbf{G} \tag{6}$$

$$\tilde{\mathbf{C}}_k = (1-\gamma)\, \hat{\mathbf{C}}_k + \gamma \mathbf{I} \tag{7}$$

The two regularization coefficients β and γ can take values between 0 and 1 ($\beta, \gamma \in [0, 1]$). The matrix $\mathbf{C}_k$is initial spatial covariance matrix of k-th class, $\mathbf{C}_k$ is regularized estimate, **I** is the identity matrix and **G** is a generic covariance matrix estimated using other subjects. Based on [48], [49], [50], and [51], whereas regularization coefficient β approximates $\mathbf{C}_k$ to generic matrix, other coefficient γ approximates to **I**. Apart from that, CSP function itself is regularized by adding a penalty term to prior condition as follows

$$J_{CSP}(\mathbf{w}) = \frac{\mathbf{w}^T \mathbf{C}_1 \mathbf{w}}{\mathbf{w}^T \mathbf{C}_2 \mathbf{w} + \alpha P(\mathbf{w})}. \tag{8}$$

In this equation, P(**w**) is the penalty function and the coefficient α represents its weight to the objective function. We refer readers to [48] for further details of CSP regularization.

Here in this study, we use Composite CSP (CCSP) and Regularized CSP with Generic Learning (GLRCSP) methods [50], [51]. We perform transfer learning by using regularized covariance matrices taken from other subjects. CCSP algorithm uses only β parameter and assigns $\alpha = \gamma = 0$. This means that it only uses generic matrix for regularization [50]. GLRCSP method uses both β and γ terms for the regularization [51].

Our dataset is comprised of actual and imagery lifting up and down motion for three weight classes. This gives us two options for regularizing the CSP filters: session-to-session transfer learning by using actual movement session on imagery session and subject-to-subject transfer learning by using imagery sessions of source subjects on the target subject.

Spatial filters are estimated using all trials of actual movement session and 80% of the motor imagery trials. Note that actual movement trials are used as if they are the source domain and motor imagery data as a target domain. The remaining 20% of the motor imagery trials are used for testing. We repeat this process for each fold and calculate the average classification accuracy for each subject. We train LDA machine learning model with the extracted spatial features from regularized CSP filters. Hence, session-to-session transfer learning is completed with regularized CSP, in which information of actual movement is transferred for the estimation of CSP filters for motor imagery data.

Alternatively, we perform subject-to-subject transfer learning between motor imagery sessions of all the subjects. For each subject, the remaining subjects are used as source domains. Next, we take 80% of the target subject's motor imagery trials to estimate CSP filters. We train LDA machine learning model with the training data and test the model on the remaining 20% trials.

D. CLASSIFICATION

The aim was to predict weight perception from EEG. After computing the features for S-T-F-TF, FSST-SVD, and RCSP, matrices of dimensions (31 subjects x 30 trials x 11 features x 16 trials) were obtained for S-T-F-TF, (31 subjects x 30 trials x 11 features x 16 trials) for FSST-SVD, and (31 subjects x 30 trials x 10 features x 16 trials) for RCSP. The feature sets provided to the classifier were resized to (31 × 30×176) for S-T-F-TF and FSST-SVD, and (31 × 30×160) for RCSP. We used a two-session paradigm which allows decoding weight perception from both actual movement and imagery sessions.

First, we used only imagination phase signals of imagery session for the interested signal area. We split our data into subsets using a subject-based approach, ''leave-one-subject-out''. Imagination phase trials from one subject were used as the test set and the remaining trials recorded from 30 subjects

were employed as the training set. We repeat this process 5 times, that is, each repetition we train a machine learning model from scratch with the training set created for that repetition and test with only the test set of that repetition. We report the average classification accuracy of 5 repetitions as final prediction score.

On the other hand, we proposed a new method that originally constructs the training dataset and test dataset of each subject to investigate the effect of the actual movement on the evaluation of the classification performance in the weight perception problem. For this purpose, the trials obtained from the imagery session of a single individual were divided into five folds, with one-fold used as the test data. Additionally, all signals from the individual's actual movement session were used in the training set. This process repeated until each fold has been used as the test data once, ensuring that the model's performance is evaluated across different subsets of the data. This procedure was repeated for each subject.

MATLAB (2019a) was used for classification. We investigated k-nearest neighbors (k-NN, k=10, distance metric was Euclidean), linear discriminant analysis (LDA), fine tree (maximum number of splits = 100, split criterion was based on Gini's diversity index), Naive Bayes (kernel type was Gaussian), and the support vector machines (SVM) with fine Gaussian kernel and quadratic kernel [66].

1) PERFORMANCE METRICS

In this study, the performance of the classification methodologies was presented using accuracy and f-measure metrics. For evaluating classification models, accuracy has the meaning of the percentage of correct prediction [66], [67]. For binary classification, it is computed using (9).

$$Accuracy = \frac{Number\ of\ correct\ predictions}{Total\ number\ of\ predictions} \tag{9}$$

Counting the number of positive class predictions that belongs to the positive class is precision and it is computed using (10). On the other hand, recall (as known as sensitivity) is a metric that the number of positive predictions out of the examples that should have been predicted as positive and computed with (11). Additionally, using the precision and recall, f-measure is calculated (12) [68].

$$Precision = \frac{\mathrm{TP}}{\mathrm{TP} + \mathrm{FP}} \tag{10}$$

$$Recall = \frac{TP}{TP + FN} \tag{11}$$

$$f - measure = 2 \times \frac{precision \times recall}{precision + recall} \tag{12}$$

III. RESULTS

The performance of machine learning approaches was examined on S-T-F-TF, FSST-SVD, and RCSP features. The classification performance was assessed using six different machine learning algorithms: SVM with Gaussian kernel, SVM with quadratic kernel, KNN, LDA, Fine Tree, and Naive Bayes. Accuracy and f-measure values were calculated as performance metrics. The features utilized, FSST-SVD and S-T-F-TF, were presented for comparison. Three binary classification scenarios were considered: light vs. heavy, light vs. medium, and heavy vs. medium.

Table 2 illustrates the classification performances of signals obtained during the Imaginary phase. According to feature comparison, the highest accuracy, reaching 70%, was achieved in distinguishing the light and medium weight classes using features obtained with FSST-SVD. In the classification comparison, the Fine Tree classifier yielded the highest accuracy, particularly in distinguishing between light and medium weights, as well as heavy and medium weights. However, the binary classification for light vs. heavy weight did not surpass the chance level (0.5).

From the results, we can clearly observe that the classification performance remains low. To overcome this problem, using the actual movement session in training data has a valuable advantage in comparison with using only the signals corresponding to imagination of lifting the object. In Table 3, we present the classification results of the proposed method in detail, using accuracy and f-measure metrics. As demonstrated in Table 2, we got the highest accuracy with the level of 80% using FSST-SVD as a feature and SVM quadratic as a classifier to discriminate medium weight and heavy objects. The proposed method has been observed to achieve a 20% increase in accuracy in distinguishing between the light and heavy weight classes and separating the heavy and medium weight classes.

1) CSP RESULTS

Here, we test classification performance of CCSP and GLRCSP. First, we train an LDA machine learning model to classify resting and imagination periods. We use features extracted from the first 5 spatial filters to create a feature vector of each trial. In Table 3 we show the classification accuracies of the top five subjects and the average classification accuracy of all subjects. We reach 78% classification performance on average with CCSP method, whereas GLRCSP reaches 72% accuracy. Classification performance varies across subjects and reaches as high as 92% accuracy.

We perform one-versus-one classification of the three classes (light, medium, heavy weights) on motor imagery data. We train an LDA machine learning model with extracted spatial features from each trial. We use all subjects except the target subject for the estimation of regularization parameters of the spatial filters. In Table 4 we show classification accuracy of the five highest subjects for each class pair (light-heavy, light-medium, medium-heavy). We also show average classification accuracy of all subjects. The results in Table 4 show that classification performance is at the chance level of 50%.

Next, we show the results of the session-to-session transfer learning approach. We use actual motor movement data from the subject to estimate regularization parameters. Then we

TABLE 2. Classification performance of the imagery session.

Class	Features	Evaluation Metrics	Classifier					
			SVMG	SVMQ	KNN	LDA	FineT	NaïveB
Light - Heavy	FSST-SVD	ACC (%)	**50**	40	50	35	50	45
		f-measure	**0.60**	0.45	0.55	0.38	0.54	0.48
	S-T-F-TF	ACC (%)	35	**50**	40	40	45	45
		f-measure	0.29	**0.66**	0.50	0.44	0.44	0.0
Light - Medium	FSST-SVD	ACC (%)	45	30	55	30	**70**	50
		f-measure	0.28	0.2	0.59	0.26	**0.62**	0.63
	S-T-F-TF	ACC (%)	50	30	45	50	40	55
		f-measure	0.1	0.53	0.57	0.26	0.2	0.0
Heavy-Medium	FSST-SVD	ACC (%)	55	35	45	40	**60**	45
		f-measure	0.26	0.13	0.44	0.29	**0.49**	0.44
	S-T-F-TF	ACC (%)	50	50	45	45	45	45
		f-measure	0.1	0.0	0.24	0.23	0.21	0.61

TABLE 3. Classification performance of the proposed method (imagery session + actual movement session).

Class	Features	Evaluation Metrics	Classifier					
			SVMG	SVMQ	KNN	LDA	FineT	NaïveB
Light - Heavy	FSST-SVD	ACC (%)	55	55	45	52	**70**	50
		f-measure	0.64	0.45	0.5	0.46	**0.68**	0.66
	S-T-F-TF	ACC (%)	55	**65**	50	60	50	45
		f-measure	0.66	**0.46**	0.61	0.52	0.47	0.58
Light - Medium	FSST-SVD	ACC (%)	50	45	50	**55**	50	40
		f-measure	0.51	0.44	0.57	**0.53**	0.6	0.08
	S-T-F-TF	ACC (%)	50	30	45	50	40	55
		f-measure	0.46	0.24	0.54	0.36	0.42	0.23
Heavy - Medium	FSST-SVD	ACC (%)	65	**80**	50	60	65	50
		f-measure	0.52	**0.82**	0.49	0.54	0.58	0.1
	S-T-F-TF	ACC (%)	45	60	55	60	60	55
		f-measure	0.23	0.58	0.42	0.55	0.56	0.23

estimate regularized CSP filters on training set of motor imagery data. We train an LDA machine learning model with the extracted spatial features and test the model on the test set from the same subject. We show the classification accuracies of the best five subjects with this approach in Table 5. With this approach, we are able to classify motor

TABLE 4. Resting vs imagery classification accuracies (%) of top five subjects.

CCSP				GLRCSP			
Subjects	**Light-Heavy**	**Light-Medium**	**Medium-Heavy**	**Subjects**	**Light-Heavy**	**Light-Medium**	**Medium-Heavy**
S08	65.00	50.00	75.00	**S30**	50.00	80.00	73.33
S22	70.00	60.00	55.00	**S08**	60.00	65.00	75.00
S09	50.00	66.67	66.67	**S19**	75.00	55.00	70.00
S20	50.00	50.00	80.00	**S05**	60.00	65.00	70.00
S26	73.33	53.33	50.00	**S15**	50.00	65.00	75.00
Average	**61.67**	**56.00**	**65.33**	**Average**	**59.00**	**66.00**	**72.67**
All Subjects	**50.83 ±12.9**	**47.94 ±11.8**	**53.39 ±12.3**	**All Subjects**	**52.28 ±11.4**	**52.89 ±11.5**	**52.56 ±12.3**

TABLE 5. One-versus-one light, medium and heavy weight classification accuracies (%) of top five subjects.

CCSP				GLRCSP			
Subjects	**Light-Heavy**	**Light-Medium**	**Medium-Heavy**	**Subjects**	**Light-Heavy**	**Light-Medium**	**Medium-Heavy**
S07	80.00	85.00	75.00	**S30**	90.00	93.33	86.67
S30	90.00	73.33	73.33	**S27**	90.00	75.00	85.00
S04	85.00	65.00	85.00	**S03**	95.00	85.00	70.00
S02	85.00	65.00	85.00	**S20**	75.00	85.00	85.00
S03	80.00	80.00	70.00	**S26**	93.33	73.33	75.00
Average	**84.00**	**73.67**	**77.67**	**Average**	**88.67**	**82.33**	**80.33**
All Subjects	**74.61 ±8.2**	**69.33 ±8.2**	**69.94 ±7.3**	**All Subjects**	**76.39 ±9.1**	**73.22 ±9.1**	**72.83 ±10.9**

imagery of different weights up to 95% accuracy. Besides, average classification performance of at least 70% accuracy is reached for each class pair.

IV. DISCUSSION

In this research paper, our primary objective was to identify distinctive features of the weight perception of the objects using EEG signals. In case of successful weight perception classification, prosthetic limb technology will take a step forward on providing *natural feeling* for the imputed people.

Different from the studies focused on weight prediction [26], [27], [28], [29], we focused on visual perception and imagination of the objects' weights, that is, the main emphasis of our study. We designed our experiment paradigm to discern and characterize motor imagery waves of the different weights (light, medium, heavy) by having two sessions; subjects performed the actual motor task movements (lifting up and putting down of the bottles) in the first session, whereas subjects only imagined the motor task of the first session in the second session.

We used FSST (Fourier-based synchrosqueezing transform) and regularized CSP (Common Spatial Patterns) methods to extract features from EEG signals. The results indicated that the FSST-SVD features representing medium and heavy objects exhibited the most distinctive characteristics as compared to the other pairwise groups. We developed a unique approach for the estimation of regularization parameters of CSP filters by employing actual motor movement trials. When binary classification problem is posed, our approach exceeded 70% classification accuracy on the prediction of objects' weights. We reached the average of 76.39%, 73.22% and 72.83% classification accuracy on light-heavy, light-medium, and medium-heavy weight class pairs respectively. We should note that for the best performing subjects, classification accuracy of our approach exceeded 90% accuracy.

Our findings shed light on a relatively unexplored area of research, as the neural correlates of weight perception have not been extensively investigated previously. Our results suggest that EEG signals indeed contain valuable information pertaining to weight perception, highlighting the potential of EEG-based approaches in the development of novel assistive technologies for individuals with upper-limb prostheses.

The integration of EEG-based weight perception estimation into prosthetic limb control systems could facilitate more seamless and intuitive interaction between the user and their device. By using neural signals, people with prosthetic limbs can feel more in tune with their movements and have better control over them. This could lead to better results in how well the limbs work and how satisfied users are with them.

On the other hand, the study also has certain limitations. One notable limitation is the relatively small sample size, the sample size was relatively small, which may affect the generalizability of the findings. Additionally, while the classification performance achieved in our study was promising, it may not be sufficient for practical applications in all cases. Furthermore, participants may encounter difficulties in performing the tasks required by the experimental paradigms, potentially affecting the quality of the EEG data collected. Environmental factors can also significantly affect EEG data quality and interpretation. External noise, such as electromagnetic interference or participant movement, can distort EEG signals, leading to inaccurate results. Moreover, variations in experimental conditions, such as lighting, temperature, or participant comfort, may introduce inconsistencies across data collection sessions. Thus, EEG signal processing can be complex. Future studies with larger and more diverse subjects, along with improved methodologies, could help address these limitations. Additionally, collaborating with industry partners or practitioners can facilitate the translation of research findings into practical applications. Engaging in co-design processes, usability testing, and iterative refinement can ensure that EEG-based technologies meet end-users' needs and preferences.

In future studies, we aim to improve utilize transfer learning approaches to further improve classification accuracy [69], [70]. We plan to adapt this approach to prosthetic design and test it first in healthy individuals and then in individuals with disabilities. Our preliminary studies demonstrate the potential of the method to be effective in such applications.

ACKNOWLEDGMENT

The authors are grateful to Gulf University for Science and Technology, Kuwait, for covering the APC for this paper, enabling its publication. *(Nedime Karakullukcu and Fatih Altindiş are co-first authors.)*

REFERENCES

[1] R. N. Scott and P. A. Parker, "Myoelectric prostheses: State of the art," *J. Med. Eng. Technol.*, vol. 12, no. 4, pp. 143–151, Jan. 1988, doi: 10.3109/03091908809030173.

[2] A. Fougner, Ø. Stavdahl, P. J. Kyberd, Y. G. Losier, and P. A. Parker, "Control of upper limb prostheses: Terminology and proportional myoelectric control—A review," *IEEE Trans. Neural Syst. Rehabil. Eng.*, vol. 20, no. 5, pp. 663–677, Sep. 2012, doi: 10.1109/TNSRE.2012.2196711.

[3] S. Chaudhary, S. Taran, V. Bajaj, and A. Sengur, "Convolutional neural network based approach towards motor imagery tasks EEG signals classification," *IEEE Sensors J.*, vol. 19, no. 12, pp. 4494–4500, Jun. 2019, doi: 10.1109/JSEN.2019.2899645.

[4] M. E. M. Mashat, C.-T. Lin, and D. Zhang, "Effects of task complexity on motor imagery-based brain–computer interface," *IEEE Trans. Neural Syst. Rehabil. Eng.*, vol. 27, no. 10, pp. 2178–2185, Oct. 2019, doi: 10.1109/TNSRE.2019.2936987.

[5] K. Djelloul and A. N. Belkacem, "EEG classification-based comparison study of motor-imagery brain–computer interface," in *Proc. Int. Conf. Recent Adv. Math. Informat. (ICRAMI)*, Sep. 2021, pp. 1–6, doi: 10.1109/ICRAMI52622.2021.9585902.

[6] D. Zapała, E. Zabielska-Mendyk, P. Augustynowicz, A. Cudo, M. Jaśkiewicz, M. Szewczyk, N. Kopiś, and P. Francuz, "The effects of handedness on sensorimotor rhythm desynchronization and motor-imagery BCI control," *Sci. Rep.*, vol. 10, no. 1, pp. 1–11, Feb. 2020, doi: 10.1038/s41598-020-59222-w.

[7] H. Sun, J. Jin, R. Xu, and A. Cichocki, "Feature selection combining filter and wrapper methods for motor-imagery based brain–computer interfaces," *Int. J. Neural Syst.*, vol. 31, no. 9, Aug. 2021, Art. no. 2150040, doi: 10.1142/s0129065721500404.

[8] N. Öztürk and B. Yilmaz, "Discrimination of rest, motor imagery and movement for brain–computer interface applications," in *Proc. Med. Technol. Nat. Congr. (TIPTEKNO)*, Nov. 2018, pp. 1–4, doi: 10.1109/TIPTEKNO.2018.8597152.

[9] M. I. Singh and M. Singh, "Development of a real time emotion classifier based on evoked EEG," *Biocybernetics Biomed. Eng.*, vol. 37, no. 3, pp. 498–509, Jan. 2017, doi: 10.1016/j.bbe.2017.05.004.

[10] R. K. Tripathy and U. Rajendra Acharya, "Use of features from RR-time series and EEG signals for automated classification of sleep stages in deep neural network framework," *Biocybernetics Biomed. Eng.*, vol. 38, no. 4, pp. 890–902, Jan. 2018, doi: 10.1016/j.bbe.2018.05.005.

[11] M. D. Luciw, E. Jarocka, and B. B. Edin, "Multi-channel EEG recordings during 3,936 grasp and lift trials with varying weight and friction," *Sci. Data*, vol. 1, no. 1, pp. 1–11, Nov. 2014, doi: 10.1038/sdata.2014.47.

[12] C. G. Lim, C. P. Soh, S. S. Y. Lim, D. S. S. Fung, C. Guan, and T.-S. Lee, "Home-based brain–computer interface attention training program for attention deficit hyperactivity disorder: A feasibility trial," *Child Adolescent Psychiatry Mental Health*, vol. 17, no. 1, p. 15, Jan. 2023, doi: 10.1186/s13034-022-00539-x.

[13] N. Karakullukcu, B. Yilmaz, and A. Y. Onver, "Real-time robotic car control using brainwaves and head movement," in *Proc. Med. Technol. Nat. Congr.*, 2018, pp. 1–4, doi: 10.1109/TIPTEKNO.2018.8596956.

[14] Z. Wang, Y. Yu, M. Xu, Y. Liu, E. Yin, and Z. Zhou, "Towards a hybrid BCI gaming paradigm based on motor imagery and SSVEP," *Int. J. Human–Computer Interact.*, vol. 35, no. 3, pp. 197–205, Feb. 2019, doi: 10.1080/10447318.2018.1445068.

[15] G. Prapas, K. Glavas, A. T. Tzallas, K. D. Tzimourta, N. Giannakeas, and M. G. Tsipouras, "Motor imagery approach for BCI game development," in *Proc. 7th South-East Eur. Design Autom., Comput. Eng., Comput. Netw. Social Media Conf. (SEEDA-CECNSM)*, Sep. 2022, pp. 1–5, doi: 10.1109/SEEDA-CECNSM57760.2022.9932937.

[16] C. Vidaurre, C. Klauer, T. Schauer, A. Ramos-Murguialday, and K.-R. Müller, "EEG-based BCI for the linear control of an upper-limb neuroprosthesis," *Med. Eng. Phys.*, vol. 38, no. 11, pp. 1195–1204, Nov. 2016, doi: 10.1016/j.medengphy.2016.06.010.

[17] W. Zhang, M. White, M. Zahabi, A. T. Winslow, F. Zhang, H. Huang, and D. Kaber, "Cognitive workload in conventional direct control vs. Pattern recognition control of an upper-limb prosthesis," in *Proc. IEEE Int. Conf. Syst. Man, Cybern. (SMC)*, Oct. 2016, pp. 002335–002340, doi: 10.1109/SMC.2016.7844587.

[18] X. Li, O. W. Samuel, X. Zhang, H. Wang, P. Fang, and G. Li, "A motion-classification strategy based on sEMG-EEG signal combination for upper-limb amputees," *J. NeuroEng. Rehabil.*, vol. 14, no. 1, pp. 1–13, Dec. 2017, doi: 10.1186/s12984-016-0212-z.

[19] A. Sun, B. Fan, and C. Jia, "Motor imagery EEG-based online control system for upper artificial limb," in *Proc. Int. Conf. Transp., Mech., Electr. Eng. (TMEE)*, Dec. 2011, pp. 1646–1649, doi: 10.1109/TMEE.2011.6199526.

[20] N. J. Limbaga, K. L. Mallari, N. R. Yeung, and J. C. Monje, "Development of an EEG-based brain-controlled system for a virtual prosthetic hand," in *Proc. IEEE Int. Conf. Bioinf. Biomed. (BIBM)*, Dec. 2022, pp. 1714–1717, doi: 10.1109/BIBM55620.2022.9995382.

[21] H. M. K. K. M. B. Herath and W. R. de Mel, "Controlling an anatomical robot hand using the brain–computer interface based on motor imagery," *Adv. Hum.-Comput. Interact.*, vol. 2021, pp. 1–15, Aug. 2021, doi: 10.1155/2021/5515759.

[22] A. Chaudhry, U. Khan, M. R. Palla, S. B. Singh, and S. V. Deshmukh, "A prosthetic arm based on electroencephalography by signal acquisition and processing on MATLAB," *Int. J. Res. Eng. Sci. Manage.*, vol. 5, no. 1, pp. 119–124, Jan. 2022. Accessed: Oct. 8, 2023.

[23] I. Faiman, S. Pizzamiglio, and D. L. Turner, "Resting-state functional connectivity predicts the ability to adapt arm reaching in a robot-mediated force field," *NeuroImage*, vol. 174, pp. 494–503, Jul. 2018, doi: 10.1016/j.neuroimage.2018.03.054.

[24] S. M. Deniz, H. Javaheri, J. F. Vargas, D. Urgun, F. Sabit, M. Tok, M. Haklidir, B. Zhou, and P. Lukowicz, "Prediction of lifted weight category using EEG equipped headgear," in *Proc. IEEE-EMBS Int. Conf. Biomed. Health Informat. (BHI)*. Greece: Institute of Electrical and Electronics Engineers Inc., Sep. 2022, pp. 1–7, doi: 10.1109/BHI56158.2022.9926744.

[25] I. M. Shuggi, H. Oh, H. Wu, M. J. Ayoub, A. Moreno, E. P. Shaw, P. A. Shewokis, and R. J. Gentili, "Motor performance, mental workload and self-efficacy dynamics during learning of reaching movements throughout multiple practice sessions," *Neuroscience*, vol. 423, pp. 232–248, Dec. 2019, doi: 10.1016/j.neuroscience.2019.07.001.

[26] M. Aslam, F. Rajbdad, and O. M. Soysal, "Weight perception analysis using electroencephalographic signals: Full/regular papers, CSCI-ISPC," in *Proc. Int. Conf. Comput. Sci.*, 2021, pp. 1678–1683, doi: 10.1109/CSCI54926.2021.00319.

[27] V. van Polanen and M. Davare, "Sensorimotor memory biases weight perception during object lifting," *Frontiers Hum. Neurosci.*, vol. 9, p. 700, Dec. 2015, doi: 10.3389/fnhum.2015.00700.

[28] Y. Chang, "Architecture design for performing grasp-and-lift tasks in brain–machine-interface-based human-in-the-loop robotic system," *IET Cyber-Physical Systems: Theory Appl.*, vol. 4, no. 3, pp. 198–203, Sep. 2019, doi: 10.1049/iet-cps.2018.5066.

[29] S. G. Chacko, P. Tayade, S. Kaur, and R. Sharma, "Creation of a high resolution EEG based brain computer interface for classifying motor imagery of daily life activities," in *Proc. 7th Int. Winter Conf. Brain-Comput. Interface (BCI)*, Feb. 2019, pp. 1–5, doi: 10.1109/IWW-BCI.2019.8737258.

[30] I. Stancin, M. Cifrek, and A. Jovic, "A review of EEG signal features and their application in driver drowsiness detection systems," *Sensors*, vol. 21, no. 11, p. 3786, May 2021, doi: 10.3390/s21113786.

[31] S. Motamedi-Fakhr, M. Moshrefi-Torbati, M. Hill, C. M. Hill, and P. R. White, "Signal processing techniques applied to human sleep EEG signals—A review," *Biomed. Signal Process. Control*, vol. 10, pp. 21–33, Mar. 2014, doi: 10.1016/j.bspc.2013.12.003.

[32] M. S. Safi and S. M. M. Safi, "Early detection of Alzheimer's disease from EEG signals using Hjorth parameters," *Biomed. Signal Process. Control*, vol. 65, Mar. 2021, Art. no. 102338, doi: 10.1016/j.bspc.2020.102338.

[33] Y. Ma, W. Shi, C.-K. Peng, and A. C. Yang, "Nonlinear dynamical analysis of sleep electroencephalography using fractal and entropy approaches," *Sleep Med. Rev.*, vol. 37, pp. 85–93, Feb. 2018, doi: 10.1016/j.smrv.2017.01.003.

[34] F. Altindis, B. Yilmaz, S. Borisenok, and K. Icoz, "Use of topological data analysis in motor intention based brain–computer interfaces," in *Proc. 26th Eur. Signal Process. Conf. (EUSIPCO)*, Sep. 2018, pp. 1695–1699, doi: 10.23919/EUSIPCO.2018.8553382.

[35] G. Pfurtscheller, "Functional brain imaging based on ERD/ERS," *Vis. Res.*, vol. 41, nos. 10–11, pp. 1257–1260, May 2001.

[36] Z. Wang, L. Cao, Z. Zhang, X. Gong, Y. Sun, and H. Wang, "Short time Fourier transformation and deep neural networks for motor imagery brain computer interface recognition," in *Concurrency Computation*. Hoboken, NJ, USA: Wiley, Dec. 2018.

[37] Y. Ma, L. Zheng, Z. Yi, Y. Xiao, C. Wang, and X. Wu, "Short-time Fourier transform covariance and selection, a feature extraction method for binary motor imagery classification," in *Proc. IEEE Int. Conf. Real-Time Comput. Robot. (RCAR)*. China: Institute of Electrical and Electronics Engineers Inc., Jul. 2021, pp. 1316–1322, doi: 10.1109/RCAR52367.2021.9517461.

[38] L. Thomas and A. K. Johnson, "Synchrosqueezing transform and its applications: A review," *Int. Res. J. Eng. Technol.*, vol. 6, no. 1, pp. 1536–1541, 2019. Accessed: Aug. 25, 2021.

[39] N. Karakullukcu and B. Yilmaz, "Detection of movement intention in EEG-based brain–computer interfaces using Fourier-based synchrosqueezing transform," *Int. J. Neural Syst.*, vol. 32, no. 1, Jan. 2022, Art. no. 2150059, doi: 10.1142/s0129065721500593.

[40] D. Degirmenci, M. Yalcin, M. A. Ozdemir, and A. Akan, "Synchrosqueezing transform in biomedical applications: A mini review," in *Proc. Med. Technol. Congr. (TIPTEKNO)*, Nov. 2020, pp. 1–5, doi: 10.1109/TIPTEKNO50054.2020.9299225.

[41] S. T. Veena and M. N. Sumaiya, "Human emotion classification using EEG signals by multivariate SynchroSqueezing transform," *Learn. Anal. Intell. Syst.*, vol. 6, pp. 179–204, Aug. 2020.

[42] O. K. Cura and A. Akan, "Classification of epileptic EEG signals using synchrosqueezing transform and machine learning," *Int. J. Neural Syst.*, vol. 31, no. 5, May 2021, Art. no. 2150005, doi: 10.1142/s0129065721500052.

[43] P. Ozel, A. Akan, and B. Yilmaz, "Synchrosqueezing transform based feature extraction from EEG signals for emotional state prediction," *Biomed. Signal Process. Control*, vol. 52, pp. 152–161, Jul. 2019, doi: 10.1016/j.bspc.2019.04.023.

[44] M. J. Antony, B. P. Sankaralingam, R. K. Mahendran, A. A. Gardezi, M. Shafiq, J.-G. Choi, and H. Hamam, "Classification of EEG using adaptive SVM classifier with CSP and online recursive independent component analysis," *Sensors*, vol. 22, no. 19, p. 7596, Oct. 2022, doi: 10.3390/s22197596.

[45] S. Zhang, Z. Zhu, B. Zhang, B. Feng, T. Yu, and Z. Li, "The CSP-based new features plus non-convex log sparse feature selection for motor imagery EEG classification," *Sensors*, vol. 20, no. 17, p. 4749, Aug. 2020, doi: 10.3390/s20174749.

[46] J. Khan, M. H. Bhatti, U. G. Khan, and R. Iqbal, "Multiclass EEG motor-imagery classification with sub-band common spatial patterns," *EURASIP J. Wireless Commun. Netw.*, vol. 2019, no. 1, pp. 1–9, Dec. 2019.

[47] P. K. Saha, Md. A. Rahman, and Md. N. Mollah, "Frequency domain approach in CSP based feature extraction for EEG signal classification," in *Proc. Int. Conf. Electr., Comput. Commun. Eng. (ECCE)*, Feb. 2019, pp. 1–6, doi: 10.1109/ECACE.2019.8679463.

[48] F. Lotte and C. Guan, "Regularizing common spatial patterns to improve BCI designs: Unified theory and new algorithms," *IEEE Trans. Biomed. Eng.*, vol. 58, no. 2, pp. 355–362, Feb. 2011, doi: 10.1109/TBME.2010.2082539.

[49] F. Lotte and C. Guan, "Spatially regularized common spatial patterns for EEG classification," in *Proc. 20th Int. Conf. Pattern Recognit.*, Aug. 2010, pp. 3712–3715, doi: 10.1109/ICPR.2010.904.

[50] H. Kang, Y. Nam, and S. Choi, "Composite common spatial pattern for subject-to-subject transfer," *IEEE Signal Process. Lett.*, vol. 16, no. 8, pp. 683–686, Aug. 2009, doi: 10.1109/LSP.2009.2022557.

[51] H. Lu, K. N. Plataniotis, and A. N. Venetsanopoulos, "Regularized common spatial patterns with generic learning for EEG signal classification," in *Proc. Annu. Int. Conf. IEEE Eng. Med. Biol. Soc.*, Sep. 2009, pp. 6599–6602, doi: 10.1109/IEMBS.2009.5332554.

[52] N. Yu, R. Yang, and M. Huang, "Deep common spatial pattern based motor imagery classification with improved objective function," *Int. J. Netw. Dyn. Intell.*, vol. 1, no. 1, pp. 73–84, 2022, doi: 10.53941/ijndi0101007.

[53] S. Ali, M. J. Ferdous, E. Hamid, and K. I. Molla, "Time-frequency coherence of multichannel EEG signals: Synchrosqueezing transform based analysis," *Int. J. Comput. Sci. Trends Technol.*, vol. 4, no. 3, pp. 40–48, 2016.

[54] P. Ofner, A. Schwarz, J. Pereira, and G. R. Müller-Putz, "Upper limb movements can be decoded from the time-domain of low-frequency EEG," *PLoS ONE*, vol. 12, no. 8, Aug. 2017, Art. no. e0182578, doi: 10.1371/journal.pone.0182578.

[55] S. Madhavan, R. K. Tripathy, and R. B. Pachori, "Time-frequency domain deep convolutional neural network for the classification of focal and non-focal EEG signals," *IEEE Sensors J.*, vol. 20, no. 6, pp. 3078–3086, Mar. 2020, doi: 10.1109/JSEN.2019.2956072.

[56] P. T. von Hippel, "Mean, median, and skew: Correcting a textbook rule," *J. Statist. Educ.*, vol. 13, no. 2, pp. 965–971, Jan. 2005, doi: 10.1080/10691898.2005.11910556.

[57] T. Trakoolwilaiwan, B. Behboodi, J. Lee, K. Kim, and J.-W. Choi, "Convolutional neural network for high-accuracy functional near-infrared spectroscopy in a brain–computer interface: Three-class classification of rest, right-and left-hand motor execution," *Neurophotonics*, vol. 5, no. 1, p. 1, Sep. 2017, doi: 10.1117/1.nph.5.1.011008.

[58] M. K. Andrade, M. A. de Santana, G. Moreno, I. Oliveira, J. Santos, M. C. A. Rodrigues, and W. P. D. Santos, "An EEG brain–computer interface to classify motor imagery signals," in *Series in BioEngineering*. Cham, Switzerland: Springer, 2020, pp. 83–98.

[59] S. Aydın, H. M. Saraoğlu, and S. Kara, "Log energy entropy-based EEG classification with multilayer neural networks in seizure," *Ann. Biomed. Eng.*, vol. 37, no. 12, pp. 2626–2630, Dec. 2009, doi: 10.1007/s10439-009-9795-x.
[60] K. P. Balanda and H. L. MacGillivray, "Kurtosis: A critical review," *Amer. Statistician*, vol. 42, no. 2, p. 111, May 1988, doi: 10.2307/2684482.
[61] J. Li and S. Sun, "Energy feature extraction of EEG signals and a case study," in *Proc. IEEE Int. Joint Conf. Neural Netw.*, Jun. 2008, pp. 2366–2370, doi: 10.1109/IJCNN.2008.4634126.
[62] P. Gonzalez-Navarro, Y. M. Marghi, B. Azari, M. Akçakaya, and D. Erdogmus, "An event-driven AR-process model for EEG-based BCIs with rapid trial sequences," *IEEE Trans. Neural Syst. Rehabil. Eng.*, vol. 27, no. 5, pp. 798–804, May 2019, doi: 10.1109/TNSRE.2019.2903840.
[63] S. Meignen, T. Oberlin, and D.-H. Pham, "Synchrosqueezing transforms: From low- to high-frequency modulations and perspectives," *Comp. Rendus. Phys.*, vol. 20, no. 5, pp. 449–460, Jul. 01, 2019, doi: 10.1016/j.crhy.2019.07.001.
[64] I. Daubechies, J. Lu, and H.-T. Wu, "Synchrosqueezed wavelet transforms: An empirical mode decomposition-like tool," *Appl. Comput. Harmon. Anal.*, vol. 30, no. 2, pp. 243–261, Mar. 2011, doi: 10.1016/j.acha.2010.08.002.
[65] K. Keng Ang, Z. Yang Chin, H. Zhang, and C. Guan, "Filter bank common spatial pattern (FBCSP) in brain–computer interface," in *Proc. IEEE Int. Joint Conf. Neural Netw.*, Jun. 2008, pp. 2390–2397, doi: 10.1109/IJCNN.2008.4634130.
[66] F. Lotte, M. Congedo, A. Lécuyer, F. Lamarche, and B. Arnaldi, "A review of classification algorithms for EEG-based brain–computer interfaces," *J. Neural Eng.*, vol. 4, no. 2, pp. R1–R13, Jun. 2007, doi: 10.1088/1741-2560/4/2/r01.
[67] Y. Li, G. Zhou, D. Graham, and A. Holtzhauer, "Towards an EEG-based brain–computer interface for online robot control," *Multimedia Tools Appl.*, vol. 75, no. 13, pp. 7999–8017, Jul. 2016, doi: 10.1007/s11042-015-2717-z.
[68] E. Zhang and Y. Zhang, "F-measure," in *Encyclopedia of Database Systems*. Cham, Switzerland: Springer, 2009, p. 1147.
[69] A. Bleuzé, J. Mattout, and M. Congedo, "Tangent space alignment: Transfer learning for brain–computer interface," *Front. Hum. Neurosci.*, vol. 16, Dec. 2022, Art. no. 1049985.
[70] F. Altindis, A. Banerjee, R. Phlypo, B. Yilmaz, and M. Congedo, "Transfer learning for P300 brain–computer interfaces by joint alignment of feature vectors," *IEEE J. Biomed. Health Informat.*, vol. 27, no. 10, pp. 4696–4706, Oct. 2023, doi: 10.1109/JBHI.2023.3299837.

NEDIME KARAKULLUKCU was born in Kayseri, Turkey, in 1993. She received the B.S. degree in biomedical engineering and the B.S. degree in mechatronics engineering from Erciyes University, Kayseri, in 2016 and 2017, respectively. She is currently pursuing the integrated Ph.D. degree in electrical and computer engineering with Abdullah Gül University, Kayseri. Since 2017, she has been a fellowship-supported Ph.D. student. Her current research interests include machine learning, brain–computer interfaces, biomedical signal processing, deep learning, and biomedical engineering.

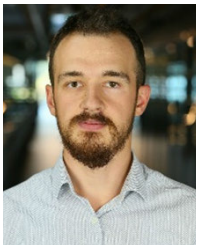

FATİH ALTINDİŞ received the B.S. degree in electrical and electronics engineering from Bilkent University, Ankara, Turkey, in 2015, and the M.S. and Ph.D. degrees in electrical and computer engineering from Abdullah Gül University, Kayseri, Turkey, in 2018 and 2023, respectively. Since 2018, he has been an Instructor. His research interests include brain–computer interfaces and EEG signal processing.

BÜLENT YILMAZ received the B.Sc. and M.Sc. degrees in electrical-electronics engineering from Middle East Technical University, Ankara, Turkey, in 1997 and 1999, respectively, and the Ph.D. degree from the Bioengineering Department, The University of Utah, Salt Lake, UT, USA. He is currently a Professor with the Electrical Engineering Department, Gulf University for Science and Technology, Hawally, Kuwait. His current research interests include biomedical signal and image processing applications on brain–computer interfaces and endoscopic images for cancer and disease assessment.